

Sonochemical Synthesis and Characterization of the Biphasic Compound $\text{Na}_2\text{Ti}_3\text{O}_7/\text{Na}_2\text{Ti}_6\text{O}_{13}$

S. M. Chaar^a, J. P. da Silva^a, F. X. Nobre^b, J. Passos^a, L. Aguilera^b, J. H. L. Silva^c,
R. S. Silva^c, F. Guerrero^d, F. M. Pontes^e, Y. Leyet^{a*}

^aUniversidade Federal do Amazonas, Departamento de Engenharia de Materiais, Laboratório de Processamento de Materiais Tecnológicos (LPMaT), Manaus, AM, Brasil.

^bUniversidade Federal do Amazonas, Departamento de Química, Programa de Pós-Graduação em Química, Manaus, AM, Brasil.

^cUniversidade Federal do Amazonas, Departamento de Física, Programa de Pós-Graduação em Física, Manaus, AM, Brasil.

^dUniversidade Federal de Sergipe, Departamento de Física, Aracaju, SE, Brasil.

^eUniversidade Estadual Paulista, Departamento de Química, Caixa Postal 473, 17033-360, Bauru, SP, Brasil.

Received: January 11, 2021; Revised: February 17, 2021; Accepted: June 16, 2021

This study processed and characterized the biphasic ceramics $\text{Na}_2\text{Ti}_3\text{O}_7/\text{Na}_2\text{Ti}_6\text{O}_{13}$ that were obtained from semi-crystalline nanoparticles synthesized using sonochemical methods. Structural characterization techniques, such as X-ray diffraction and Raman spectroscopy, were used to identify the crystalline phases present. The Rietveld refinement revealed, among other structural parameters, the presence of two crystalline phases in compositions of 55.90% and 44.10% for sodium hexatitanate and trititanate, respectively. Via Raman spectroscopy, the presence of the main vibrational modes that correspond to the phases present in biphasic ceramics was confirmed. Finally, by using complex impedance spectroscopy, a decrease in the electrical resistance of both the grain ($10^6 \Omega$ - $10^4 \Omega$) and its boundary ($10^8 \Omega$ - $10^5 \Omega$) under increasing temperature was identified.

Keywords: Biphasic ceramics $\text{Na}_2\text{Ti}_3\text{O}_7/\text{Na}_2\text{Ti}_6\text{O}_{13}$, sonochemical method, Rietveld refinement, complex impedance spectroscopy.

1. Introduction

The main phases, trititanate and hexatitanate, ($\text{Na}_2\text{Ti}_3\text{O}_7$ and $\text{Na}_2\text{Ti}_6\text{O}_{13}$) of the sodium titanate family have been extensively studied in recent years due to their interesting physical and chemical properties^{1,2}. These phases present, as a fundamental structural characteristic, a monoclinic crystalline structure, however there is a variation in the shape and position in which the Na^+ ion appears with the oxygen. This leads to structural organization in the layers for $\text{Na}_2\text{Ti}_3\text{O}_7$ and the tunnels for $\text{Na}_2\text{Ti}_6\text{O}_{13}$ ^{1,2}. These characteristics make the trititanate interesting from the point of view of its electrical properties, since it has a higher density of charge carriers¹. In the case of hexatitanate, the tunnel shape of its crystalline structure facilitates the presence of a large number of conduction paths³. Recently, several studies have been published revealing the electrical characteristics of ceramics in both the crystalline phases^{1,3-5}. However, there is very little information in the literature from the point of view of their electrical properties and what occurs in sodium titanate ceramics that have phase mixtures.

It is an empirical fact that the obtaining and methods of synthesis used are very important, since these directly influence

the properties of the material produced. The sonochemical synthesis method has numerous advantages that include high performance, simplicity and the possibility of obtaining materials with particle sizes in the order of nanometers⁶. As a result, the number of studies reporting the sonochemical synthesis has been increasing. Recently, the use of sonochemical synthesis to produce materials belonging to the sodium titanate family has been reported for the first time^{4,5}. In these studies, structural and electrical details of the ceramics produced were revealed, but only from one crystalline phase or another. As far as we know, there are still no studies that reveal the structural and electrical details of biphasic ceramic samples with a phase composition of hexatitanate and 50% trititanate.

Taking the issues previously stated into account, this study aimed, via sonochemistry, to synthesize biphasic ceramics of $\text{Na}_2\text{Ti}_3\text{O}_7$ and $\text{Na}_2\text{Ti}_6\text{O}_{13}$ with 50% phase composition and perform their electrical characterization.

2. Experimental

The reagents used in the synthesis were titanium isopropoxide ($\text{C}_{12}\text{H}_{28}\text{O}_4\text{Ti}$, Sigma-Aldrich, 97%), isopropyl

*e-mail: yurileyet@yahoo.es

alcohol (C_3H_8O , Synth) and a 1 mol L⁻¹ sodium hydroxide solution (NaOH, Synth, purity > 98%). Using an ultrasonic processor (Sonics Vibra-Cell model VCX 750), the reagent solution was subjected to a burst of ultrasonic irradiation of 487.5 W for 15 minutes at room temperature. No additional treatment of the precursors was necessary due to their degree of analytical purity. After sonication, the material was dried in an oven for 12 hours at 110 °C, and part of the material was subjected to heat treatment in a muffle furnace at 900 °C for 1 hour.

The structural analysis, via X-ray diffraction (XRD), was performed in a diffractometer (Empyrean, Malvern Panalytical), whose operating parameters were as follows: monochromatic copper radiation ($K\alpha = 1.54 \text{ \AA}$), 40 kV voltage, 40 mA current and variation diffraction angle 2θ from 5° to 100°. The Raman spectroscopy analyses used a spectrometer (inVia Qontor, Renishaw) with lens attached directly to a vertical microscope that had a focal length of 250 mm, detection in the spectral range of 200 to 1064 nm, excitation laser of 532 nm and variation in the number of wavelengths from 100 to 1200 cm⁻¹. The adjustment of the Raman spectra was performed by analyzing the oscillation bands shown in the Igor Pro analysis program.

Scanning electron microscopy (SEM) images were obtained (VEGA3, TESCAN) at a voltage of 15 kV. Finally, for electrical characterization, samples of 6 mm diameter and 1 mm thickness were prepared, and were sintered at 950 °C for 2 hours without previous heat treatment, i.e., from the semicrystalline phase. The measurements were performed on an impedance analyzer (1260, Solartron) coupled with a dielectric interface (1296A, Solartron), in an isothermal regime, by first varying the frequency of the applied electric field (500 mV). Subsequently, measurements were made at different temperature values.

3. Results and Discussion

3.1. X-ray diffraction pattern and structural Rietveld refinement

Figure 1a, b shows the X-ray diffraction pattern of NaTTs for comparison with the standard diffraction pattern of $Na_2Ti_3O_7$ and $Na_2Ti_6O_{13}$, as well as the structural Rietveld refinement plot.

Based on the diffraction pattern of the NaTTs sample (Figure 1a), high intensity and narrow peaks can be seen that suggest a high degree of crystallinity and order/disorder at a short and long-range^{1,5}. These peaks were indexed using the X'pert HighScore Plus version 2.0a, for Windows, which confirmed the presence of phase mixture of the sodium titanate polymorphs. Therefore, the NaTTs sample is composed of disodium phyllo-heptaotrititanate ($Na_2Ti_3O_7$), which exhibits a monoclinic structure ($P121/m1$) with two formulas per unit cell ($Z = 2$) and relates to the inorganic crystal structure database (ICSD) card n°. 15463⁷. In addition, the disodium hexatitanate ($Na_2Ti_6O_{13}$) relates to the ICSD card n°. 23877 and monoclinic structure ($C12/m1$) with two formulas per unit cell⁸.

The detailed study regarding the phase composition and the unit cell parameters was performed using the Rietveld

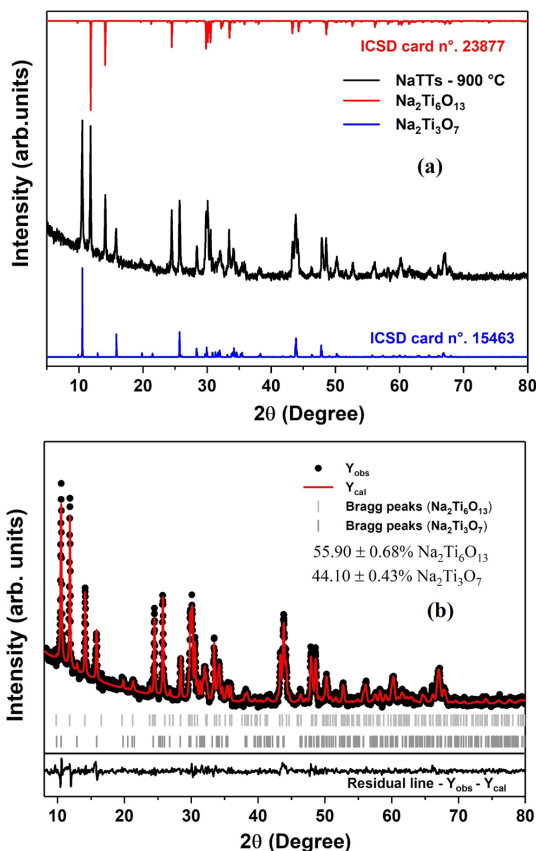


Figure 1. (a) XRD pattern of NaTTs sintered at 900 °C and standard XRD pattern of $Na_2Ti_6O_{13}$ (ICSD card n°. 15463) and $Na_2Ti_3O_7$ (ICSD card. n°. 23877) and (b) their structural Rietveld refinement plot.

refinement method via the FullProf package software⁹. The lattice parameters (a , b , c , α , β , γ), unit cell volume (V) atomic coordinates (x , y , z), background, Cagliote parameters of Pseudo-Voigt function (U , V and W), thermal anisotropic factor (B_{iso}) and occupation, O_{cc} were also refined^{1,10-15}. The quality of computed data was checked using R quality indicators (R_{exp} , R_p , R_{wp} and χ^2), as well as the profile of the residual line ($Y_{obs} - Y_{cal}$)¹⁶. The residual line was obtained through the difference between the intensity of peaks from the experimental data (Y_{obs}), contained in the diffraction pattern of the NaTTs samples, and the theoretical intensities (Y_{cal}) of the XRD peaks from the standard ICSD card for the $Na_2Ti_3O_7$ (ICSD card n°. 15463) and $Na_2Ti_6O_{13}$ (ICSD card n°. 23877) structures.

Based on Figure 1b, it can be confirmed that there is phase mixture of the sodium titanate, and the XRD diffraction pattern of the NaTTs sample is in accordance with the theoretical diffraction peaks of $Na_2Ti_3O_7$ and $Na_2Ti_6O_{13}$. Although there are small differences in the XRD peaks in the interval from $2\theta = 5^\circ$ to 20° , this is probably associated with the method of synthesis, particle size, structural defects, vacancies, and phase mixture^{1,5}. Morgado et al.¹⁷ linked the phase conversion dependence of sodium titanate nanotubes to anatase, rutile, hexatitanate and trititanate with an increase in the temperature of thermal treatment, by using the structural analysis of Rietveld refinement. The authors confirmed that

the occurrence of structural defects and vacancies are the main factors in the instability that, consequently, led to the conversion of them.

According to the Rietveld refinement results shown in Table 1 and S1, it can be noted that all refined parameter values are acceptable and very close to those contained in the ICSD database cards n°. 15463 and 23877, and correspond to Na₂Ti₃O₇ and Na₂Ti₆O₁₃, and in the literature^{18,19}. In addition, the chi-square parameter (χ^2) was equal to 1.89, indicating the best correlation for adjustment of computed data, due to this being less than 2²⁰. Regarding the phase composition, the percentage of Na₂Ti₃O₇ and Na₂Ti₆O₁₃ are 44.11 ± 0.43% and 55.89 ± 0.68%, respectively.

Where k is the shape factor constant, in this study, the spherical shape of particles is adopted ($k = 0.9$), λ_{Cu} is the wavelength of copper irradiation ($CuK\alpha = 1.54 \text{ \AA}$) and the θ

is the Bragg angle of each diffraction peak. The corrected full width at half maximum (B_{tot}) was obtained from the Rietveld refinement, where the instrumental contribution (B_{ins}) is corrected using the XRD pattern of lanthanum hexaboride (LaB₆) as the standard diffraction pattern.

The average crystallite size (D_{hkl}) was determined using the Scherrer equation²¹ as follows:

$$D_{hkl} = \frac{k_{Cu}}{B_{Tot} * \cos\theta} \quad (1)$$

The D_{hkl} for Na₂Ti₃O₇ and Na₂Ti₆O₁₃ contained in the NaTTs sample were 34.62(4) nm and 28.99(6) nm, respectively. Sodium titanate nanotubes have been studied by Morgado et al.²¹ who, using the Scherrer method, determined the crystallite size of Na₂Ti₆O₁₃ in the range from 32.0 ± 1.1 nm to 100.1 nm. However, particles with a size of between 40 to 90 nm are reported by Kulova et al.²² for Na₂Ti₃O₇ after 35 charge/discharge cycles on electrochemistry experiments. Thus, these values are close to the values found in this study.

Table 1. Structural Rietveld refinement results obtained for NaTTs sample and contained in the ICSD card n°. 15463 (Na₂Ti₃O₇) and n°. 23977 (Na₂Ti₆O₁₃) as standard structures.

Parameters	NaTTs sample	ICSD card n°. 15463	ICSD card n°. 23877
<i>Na₂Ti₃O₇</i>			
a (Å)	8.577	8.571(2)	-
b (Å)	3.795	3.804(2)	-
c (Å)	9.1360	9.135(2)	-
α (°)	90.000	90.000	-
β (°)	101.54	101.57(5)	-
γ (°)	90.000	90.000	-
V (Å ³)	291.36	291.79(19)	-
D_{hkl} (nm)	34.62(4)	-	-
Z	2	2	-
D_x (g cm ⁻³)	3.622	-	-
Xr (%) + SD	44.11(0.43)	-	-
χ^2	1.89	-	-
<i>Na₂Ti₆O₁₃</i>			
a (Å)	15.127	-	15.131(2)
b (Å)	3.745	-	3.745(2)
c (Å)	9.162	-	9.159(2)
α (°)	90.000	-	90.000
β (°)	99.09	-	99.30(5)
γ (°)	90.000	-	90.000
V (Å ³)	512.57(22)	-	512.18(31)
D_{hkl} (nm)	28.99(6)	-	-
Z	2	-	2
Xr (%) + SD	55.89(0.68)	-	-
D_x (g cm ⁻³)	3.543	-	-
χ^2	0.89	-	-

Legend: Xr = fraction of each phase (%); V = unit cell volume; Z = formula per unit cell; D_x = density; χ^2 = chi-square.

3.2. Characterization by Raman Spectroscopy.

Raman spectra of the NaTTs samples with and without heat treatment at 900 °C are shown in Figure 2. They have a high number of defined peaks; 28 vibrational modes per spectrum. These characteristics suggest a better crystallinity and larger particle sizes compared to the sodium titanate nanostructures reported in the literature, with few broad bands in their Raman spectra²³⁻²⁷. The determination of the number of modes, as well as their respective Raman shifts in cm⁻¹, was carried out through the adjustment with oscillator curves in the Igor Pro analysis program (Figure 3).

Regarding the sample after the sonochemical synthesis, the presence of the Na₂Ti₃O₇ phase can be associated with modes 117, 303, 344, 588, 847 and 883 cm⁻¹^{22,28,29} and that of the Na₂Ti₆O₁₃ phase, with modes 328, 362, 393, 526, 606 and 868 cm⁻¹²⁹⁻³¹. However, it should be noted that most of the vibrational modes in this sample are also compatible with other structures such as β -Na₂TiO₃, γ -Na₂TiO₃ and

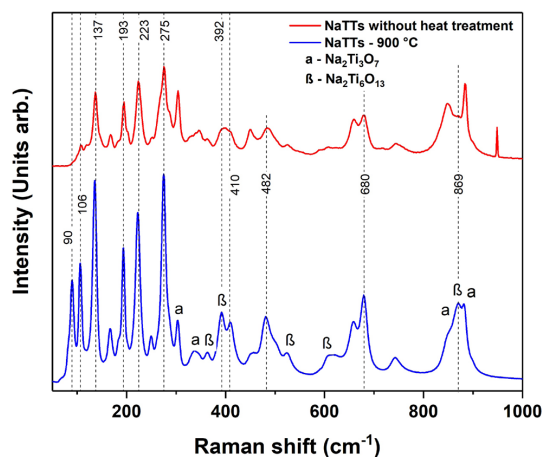


Figure 2. Raman spectra of sodium titanate samples with and without heat treatment.

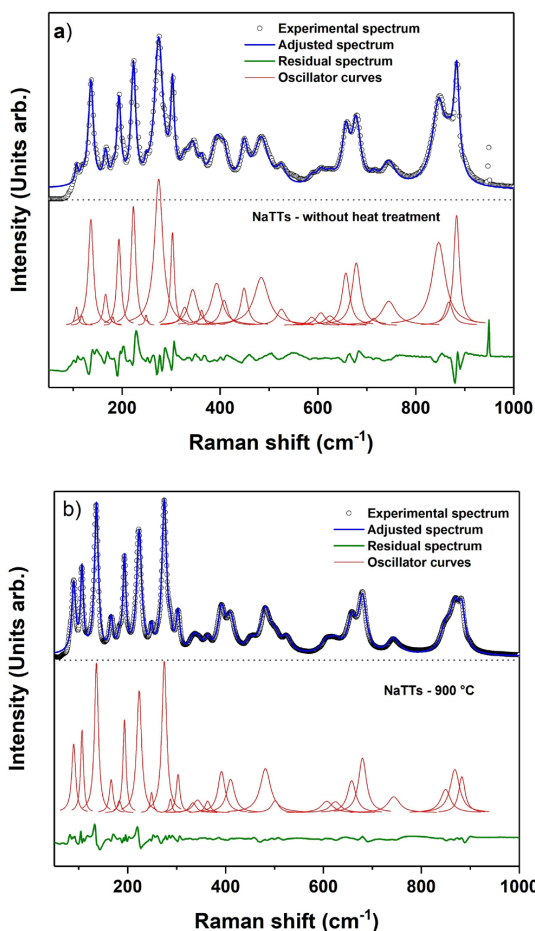


Figure 3. Raman spectra adjustment of NaTTs samples without heat treatment (a) and with heat treatment (b) using the Igor Pro program.

$\text{Na}_8\text{Ti}_5\text{O}_{14}$ ²⁹. Nevertheless, the presence of these phases was not determined by XRD.

The spectrum of the heat-treated sample also indicates a mixture of the phases $\text{Na}_2\text{Ti}_3\text{O}_7$ and $\text{Na}_2\text{Ti}_6\text{O}_{13}$ ^{23,29,32,33}. This corroborates the result obtained by the XRD analysis presented above.

Some alterations can be observed when comparing the two spectra, such as the appearance of the 90 cm^{-1} mode and the intensity increase in the $106, 137, 193, 224, 275, 392, 410, 482, 680$ and 869 cm^{-1} bands. These modifications may be a result of the heat treatment itself, since the temperature of $900\text{ }^\circ\text{C}$ favors the material crystallization and the $\text{Na}_2\text{Ti}_6\text{O}_{13}$ phase formation³⁴.

Based on the study carried out by F.L.R. e Silva et al.²⁸, the following four characteristic bands of $\text{Na}_2\text{Ti}_3\text{O}_7$ can be identified: a band at 850 cm^{-1} , attributed to Ti-O bond stretchings, and the bands $303, 343$ and 883 cm^{-1} , which are related to different types of O-Ti-O bond vibrations. The peaks referring to $\text{Na}_2\text{Ti}_6\text{O}_{13}$ are located at $333, 363, 392, 524, 607$ and 869 cm^{-1} ²⁹⁻³¹. The most energetic bands, 869 and 883 cm^{-1} , correspond to vibrations of the shortest Ti-O bonds in the $\text{Na}_2\text{Ti}_6\text{O}_{13}$ and $\text{Na}_2\text{Ti}_3\text{O}_7$ structures, respectively³³.

Another fourteen vibrational modes were obtained from the heat treatment at $90, 106, 136, 166, 194, 224, 249, 275,$

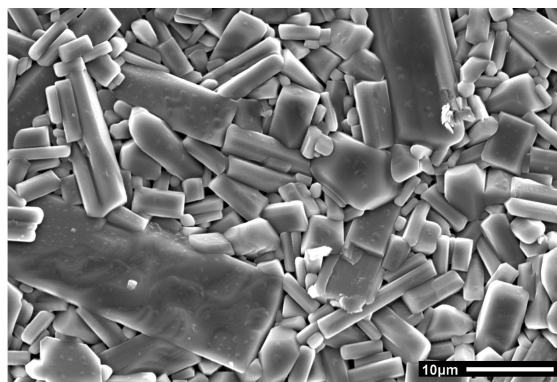


Figure 4. SEM image corresponding to a biphasic sample $\text{Na}_2\text{Ti}_3\text{O}_7/\text{Na}_2\text{Ti}_6\text{O}_{13}$, sintered from the semi-crystalline phase at $950\text{ }^\circ\text{C}$ for 2h.

$410, 451, 482, 658, 680$ and 744 cm^{-1} . However, it is not possible to identify them due to the proximity of the energy values described in the literature for the phases of $\text{Na}_2\text{Ti}_3\text{O}_7$ and $\text{Na}_2\text{Ti}_6\text{O}_{13}$. The peaks at 657 and 680 cm^{-1} ^{28,31,32} are related to movements of titanium and oxygen bonds, while the 194 cm^{-1} mode may be associated with sodium ions (Na^+). One band, around 275 cm^{-1} , can be attributed to dislocations of Na-O-Ti bonds for the $\text{Na}_2\text{Ti}_6\text{O}_{13}$ phase³² or O-Ti-O bonds of the $\text{Na}_2\text{Ti}_3\text{O}_7$ phase²⁸. According to Y. Xu et al. and M. Shirpour et al.^{26,33}, generally the vibrations related to the sodium are in the region below 400 cm^{-1} and the displacements relative to the TiO_6 octahedrons are above 600 cm^{-1} .

Figure 4 shows the microstructure of the sample in ceramic form after sintering. As can be seen in this image, there are grains with elongated, bar-shaped formats and with a large size distribution. However, from this figure it is not possible to distinguish the grains that correspond to one or another phase. This is because, as mentioned above, these phases are isomorphous. Similar results were previously reported^{3,4,13}.

3.3. Electrical characterization of the biphasic ceramic sample

As previously mentioned, the complex impedance spectroscopy technique was used to perform the electrical characterization of the sample in question. Figure 5 shows the Cole-Cole diagram, which corresponds to the relationship between the real and imaginary part of the complex impedance that is measured at different frequencies and temperatures. The curves corresponding to the highest temperature values were inserted in the lower right edge, in order to be more clearly visualized. As can be seen, there is a decrease in the diameter of the semicircles as the temperature rises to two orders of magnitude. This is associated with a conductive process that may be being thermally activated³⁵. In this case, the diameter of the semicircles corresponds to the total resistance (R_t) of the sample. This R_t can be determined by adjustment with an equivalent circuit, and obtains the resistance corresponding to the grain and its boundary³.

Figure 6 shows the behavior of the resistance that corresponds to the grain and grain boundary as a result of temperature, and was obtained from the adjustment using the equivalent circuit model, as shown in the previous figure. The errors in determining these values were less than 5%. Note that the

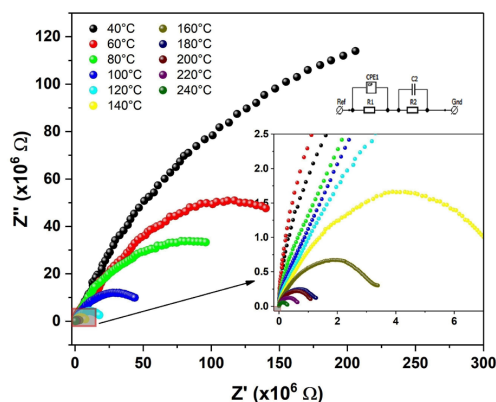


Figure 5. Cole–Cole diagrams corresponding to a biphasic sample $\text{Na}_2\text{Ti}_3\text{O}_7/\text{Na}_2\text{Ti}_6\text{O}_{13}$, sintered from the semi-crystalline phase at 950 °C for 2 h. Inset: Equivalent circuit model used.

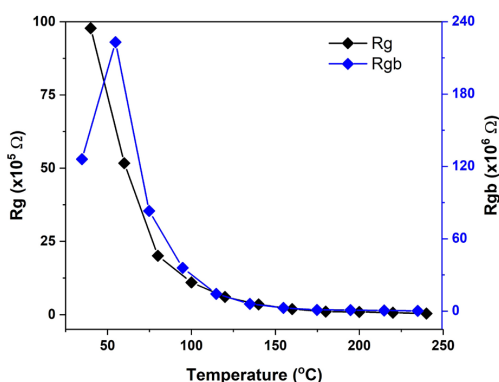


Figure 6. R_g and R_{gb} , calculated using an equivalent circuit model, as a function of the temperature.

behavior presented for both quantities is the same, but has a decrease in resistance values with increasing temperature, which is typical of insulating materials. However, it should be noted that there is a difference of an order of magnitude between R_g (less resistive) and R_{gb} (more resistive). This can be justified if it is considered that the grain region is structurally homogeneous, and more semi-conductive.

In the grain boundary, impurities accumulate resulting in a very anisotropic and therefore more insulative region. This behavior results in the prevalence of the behavior of the grain boundary region in the electrical response of this material. The values of electrical resistance obtained in this work for both the grain region and the grain boundary region are slightly higher than those previously reported for materials with pure phase of one or another phase when obtained by sonochemical synthesis^{3,4}. Among the possible causes that originated this behavior, the non-optimization in the synthesis and sintering parameters of this biphasic material can be considered. Another factor that could have contributed to this result is that, for the percentages of phases achieved, there is a relationship between the density of the load carriers and the conduction paths that does not favor charge mobility.

4. Conclusions

$\text{Na}_2\text{Ti}_3\text{O}_7/\text{Na}_2\text{Ti}_6\text{O}_{13}$ biphasic ceramics were successfully obtained from semi-crystalline nanoparticles using sonochemical methods. Via the XRD technique, the presence of two phases with monoclinic structure was identified. However, these presented spatial groups (P121/m1) and (C12/m1) that correspond to sodium trititanate and hexatitanate. The Rietveld refinement allowed us to determine the phase composition that corresponds to a percentage of 55.9% for hexatitanate and 44.1% for sodium trititanate. By confirming the vibrational modes obtained using Raman spectroscopy, the presence of both crystalline phases in the sample was confirmed. Finally, complex impedance spectroscopy revealed details of the electrical behavior of the biphasic sample. There was a decrease in the electrical resistance of both the grain ($10^6 \Omega$ - $10^4 \Omega$) and its boundary ($10^8 \Omega$ - $10^5 \Omega$) with the increasing temperature.

5. Acknowledgments

The authors would like to thank Fundação de Amparo a Pesquisa do Estado do Amazonas (FAPEAM) contract number 062.00939/2019. This study was financed in part by the Coordenação de Aperfeiçoamento de Pessoal de Nível Superior - Brazil (CAPES) - Finance Code 001.

6. References

- Basilio LAL, Xavier F, Sales JCC Jr, Andrade JCS, Anglada-Rivera JA, Aguilera L, et al. Fast synthesis of $\text{Na}_2\text{Ti}_3\text{O}_7$ system synthesized by microwave-assisted hydrothermal method: electrical properties. *Ceram Int.* 2020;46(15):23834-9.
- Cech O, Castkova K, Chladil L, Dohnal P, Cudek P, Libich J, et al. Synthesis and characterization of $\text{Na}_2\text{Ti}_6\text{O}_{13}$ and $\text{Na}_2\text{Ti}_6\text{O}_{13}/\text{Na}_2\text{Ti}_3\text{O}_7$ sodium titanates with nanorod-like structure as negative electrode materials for sodium-ion batteries. *J. Energy Storage.* 2017;14:391-8.
- Aguilera L, Fagundes N, Melo AD, Bandeira B, Nobre FX, Anglada-Rivera J, et al. Influence of sonication time on the structure and electrical properties of $\text{Na}_2\text{Ti}_6\text{O}_{13}$ ceramics: an approach applying the Mott-Schottky model. *Ceram Int.* 2020;46:8706-10.
- Leyet Y, Guerrero F, Anglada-Rivera J, de Souza RFB, Brito WR, Aguilera L, et al. Synthesis of $\text{Na}_2\text{Ti}_3\text{O}_7$ nanoparticles by sonochemical method for solid state electrolyte applications. *J Solid State Electrochem.* 2018;22:1315-9.
- Fagundes NG, Nobre FX, Basilio LAL, Melo AD, Bandeira B, Sales JCC, et al. Novel and simple way to synthesize $\text{Na}_2\text{Ti}_6\text{O}_{13}$ nanoparticles by sonochemical method. *Solid State Sci.* 2019;88:63-6.
- Vijaya Kumar R, Diamant Y, Gedanken A. Sonochemical synthesis and characterization of nanometer-size transition metal oxides from metal acetates. *Chem Mater.* 2000;12:2301-5.
- Andersson S, Wadsley AD. The crystal structure of $\text{Na}_2\text{Ti}_3\text{O}_7$. *Acta Crystallogr.* 1961;14:1245-9.
- Andersson S, Wadsley AD. The structures of $\text{Na}_2\text{Ti}_6\text{O}_{13}$ and $\text{Rb}_2\text{Ti}_6\text{O}_{13}$ and the alkali metal titanates. *Acta Crystallogr.* 1962;15:194-201.
- Rodriguez-Carvajal J. Magnetic structure determination from powder diffraction using the program *FullProf*. *J Appl Crystallogr.* 2001;30:6.
- Sousa GS, Nobre FX, Júnior EAA, Bezerra RDS, de Sá ML, de Matos JME, et al. Photocatalytic performance of $\beta\text{-Ag}_2\text{MoO}_4$ microcrystals at different experimental conditions. *Environ Nanotechnol Monit Manag.* 2020;14:100379.

11. Nobre FX, Gil Pessoa WA, Ruiz YL, Imbiriba Bentes VL, Silva-Moraes MO, Costa Silva TM, et al. Facile synthesis of nTiO₂ phase mixture: characterization and catalytic performance. *Mater Res Bull.* 2019;109:60-71.
12. Wu C, Hua W, Zhang Z, Zhong B, Yang Z, Feng G, et al. Design and synthesis of layered Na₂Ti₃O₇ and tunnel Na₂Ti₆O₁₃. *Adv Sci.* 2018;5:1800519.
13. Chandel S, Lee S, Lee S, Kim S, Pal Singh S, Kim J, et al. Rai Hierarchically nanorod structured Na₂Ti₆O₁₃/Na₂Ti₃O₇ nanocomposite as a superior anode for high-performance sodium ion battery. *J Electroanal Chem (Lausanne Switz).* 2020;877:114747.
14. Nobre FX, Nogueira IC, Souza GS, Matos JME, Couceiro PRC, Brito WR, et al. Structural and optical properties of Ca_{0.9}Cu_{0.01}WO₄ solid solution synthesized by sonochemistry method at room temperature. *Inorg Chem.* 2020;59:6039-46.
15. Nobre FX, Muniz R, Martins F, Silva BO, de Matos JME, da Silva ER, et al. Calcium molybdate: toxicity and genotoxicity assay in *Drosophila melanogaster* by SMART test. *J Mol Struct.* 2020;1200:1270962.
16. Campos WEO, Nobre FX, Rocha GNR Fo, Silva MAR, Costa CEF, et al. High photocatalytic activity under visible light for a new morphology of Bi₂WO₆ microcrystals. *Catalysts.* 2019;9:667.
17. Morgado E, de Abreu MAS, Pravia ORC, Marinkovic BA, Jardim PM, Rizzo FC, et al. A study on the structure and thermal stability of titanate nanotubes as a function of sodium content. *Solid State Sci.* 2006;8:888-900.
18. Naeyaert PJP, Avdeev M, Sharma N, Ben Yahia H, Ling CD. Synthetic, structural, and electrochemical study of monoclinic Na₄Ti₅O₁₂ as a sodium-ion battery anode material. *Chem Mater.* 2014;26:7067-72.
19. Manfroi DC, Cavalheiro AA, Perazolli LA, Varela JA, Zaghete MA. Titanate nanotubes produced from microwave-assisted hydrothermal synthesis : photocatalytic and structural properties. *Ceram Int.* 2014;40:14483-91.
20. Toby BH. R factors in Rietveld analysis: how good is good enough? *Powder Diffr.* 2006;21:67-70.
21. Morgado E, de Abreu MAS, Moure GT, Marinkovic BA, Jardim PM, Araujo AS. Effects of thermal treatment of nanostructured trititanates on their crystallographic and textural properties. *Mater Res Bull.* 2007;42:1748-60.
22. Kulova TL, Kudryashova YO, Kuz AA, Skundin AM, Stenina IA, Chekannikov AA. Study of degradation of Na₂Ti₃O₇ - based electrode during cycling. *J Solid State Electrochem.* 2019;23:455-63.
23. Viana BC, Ferreira OP, Souza Filho AG, Mendes Filho J, Alves OL. Structural, Morphological and Vibrational Properties of Titanate Nanotubes and Nanoribbons. *J Braz Chem Soc.* 2009;20:167-75.
24. Viana BC, Ferreira OP, Filho AGS, Hidalgo AA, Filho JM, Alves OL. Alkali metal intercalated titanate nanotubes: A vibrational spectroscopy study. *Vib Spectrosc.* 2011;55:183-7.
25. Zhang Z, Goodall JBM, Brown S, Karlsson L, Clark RJH, Hutchison JL, et al. Continuous hydrothermal synthesis of extensive 2D sodium titanate. *R. Soc. Chem.* 2010;39:711-4.
26. Xu Y, Bauer D, Lübke M, Ashton TE, Zong Y, Darr JA. High-power sodium titanate anodes; a comparison of lithium vs sodium-ion batteries. *J Power Sources.* 2018;408:28-37.
27. Leite MM, Martins VL, Vichi FM, Torresi RM. Electrochemistry of sodium titanate nanotubes as a negative electrode for sodium-ion batteries. *Electrochim Acta.* 2020;331:135422.
28. Silva FLR, Araújo AAF, Silva MB, Balzuweit K, Bantignies JL, Caetano EWS, et al. Polarized Raman, FTIR, and DFT study of Na₂Ti₃O₇ microcrystals. *J Raman Spectrosc.* 2018;49:538-48.
29. Bamberger CE, Begun GM. Sodium titanates: stoichiometry and raman spectra. *J Am Ceram Soc.* 1987;70:C-48-51.
30. Zárate RA, Fuentes S, Cabrera AL, Fuenzalida VM. Structural characterization of single crystals of sodium titanate nanowires prepared by hydrothermal process. *J Cryst Growth.* 2008;310:3630-7.
31. Su Y, Lou Balmer M, Bunker BC. Raman spectroscopic studies of silicotitanates. *J Phys Chem B.* 2000;104:8160-9.
32. Zhang Q, Zhang T, Wei Y, Zhai T, Li H. Removing structural water from sodium titanate anodes towards barrier-free ion diffusion for sodium ion batteries †. *J Mater Chem A Mater Energy Sustain.* 2017;5:18691-7.
33. Shirpour M, Cabana J, Doeff M. New materials based on a layered sodium titanate for dual electrochemical Na and Li intercalation systems. *Energy Environ Sci.* 2013;6:2538-47.
34. Dynarowska M, Kotwiński J, Leszczynska M, Marzantowicz M, Krok F. Ionic conductivity and structural properties of Na₂Ti₃O₇ anode material. *Solid State Ion.* 2017;301:35-42.
35. Padurariu L, Lukacs A, Stoian G, Lupu N, Curecheriu LP. Scale-dependent dielectric properties in BaZr_{0.05}Ti_{0.95}O₃ ceramics. *Materials.* 2020;13(19):4386.

Supplementary material

The following online material is available for this article:

Table S1 - Structural Rietveld refinement results for atomic coordinates, site and wyckoff of NaTTs contained on ICSD cards n°. 15463 and 23877.